# Computer-Aided Analysis of Cassegrain Antennas

By H. ZUCKER and W. H. IERLEY

(Manuscript received December 8, 1968)

*A method of analyzing, in detail, the performance of symmetrical Cassegrain antennas has been developed that uses a digital computer efficiently. For a specified antenna geometry and feed excitation, the program will compute and graphically display the amplitude and phase illumination of the subreflector, main reflector, and far-field pattern. These results may be used to optimize antenna performance by changing parameters and observing the effect.*

*Analysis of a Cassegrain antenna with a near-field conical horn feed is discussed as an application of the method. Because the radiation characteristics of the horn are determined by the horn flare angle rather than the horn aperture, broadband performance is obtained. It was indeed found that a 50 per cent bandwidth is achieved with a dual mode $TE_{11} - TM_{11}$ mode feed, provided the proper phase relationship between the modes can be maintained over the band. For dual mode excitation an aperture efficiency of 70% and a noise temperature due to the power loss at the sub and main reflectors of less than 6.5°K was obtained. For a single mode feed ($TE_{11}$), there was a degradation in the E-plane side lobe levels and a corresponding 10°K increase in noise temperature. Excitation in the $TM_{01}$ mode was also examined for angle-error sensing purposes. Also, the antenna can be used with reasonable efficiency well below the design frequency in which case it functions as a far-field fed Cassegrain antenna.*

## I. INTRODUCTION

The essential radiation characteristics of multiple reflector antennas can be predicted very accurately with existing analytical and computational methods. Previous work on the open Cassegrain antenna showed that good agreement can be achieved between calculated and experimental results.[1] Deviations occurred mainly in the sidelobe regions of the radiation patterns, and these had only a small effect on overall antenna performance.

We are concerned here with a simpler problem, but one of perhaps more general interest: the analysis of symmetrical Cassegrain antennas. We present a computational method in which the amplitude and phase illuminations of the subreflector and main-reflector, as well as the far-field radiation pattern, are determined in detail, given the geometry of the antenna, the dimensions of the feed horn, and the excitation modes of the feed. The analysis includes near-field excitation—an important configuration for broadband operation. Included in the program is a graphic routine which plots all radiation patterns, the intermediate illuminations and the final far-field results. Because of the this feature, and the fact that only seven parameters are required to define the geometry of the antenna, the program is particularly useful for optimizing antenna performance.

The symmetry of the antenna results in improved computational efficiency. For the open Cassegrain antenna, double-integration was required to compute radiation patterns. An approximation recently was obtained[2] which, when applied to symmetrical Cassegrain antennas, eliminates one integration with only a small reduction in accuracy.[2] This makes it possible to compute the radiation characteristics of large Cassegrain antennas a few hundred wavelengths diameter in minutes.

## II. NEAR-FIELD SYMMETRIC CASSEGRAIN ANTENNA

The antenna under consideration was intended to be used as the ground station of a satellite communications system. Wide-bandwidth (25 per cent) and low-noise requirements motivated the choice of a near-field conical-horn symmetric Cassegrain configuration. The near-field feed produces relatively low spillover at the subreflector, resulting in a lower noise temperature.[3] Also, because radiation of the feed is virtually confined to the geometrical illumination region of the horn,[4] there is a larger potential bandwidth available.

An additional requirement had to be explored: operation at about ¼ nominal frequency, for target-acquisition, by using both $TE_{11}$ and $TM_{01}$ mode excitation. This leads to the choice of a near-field design at the higher frequency because it would tend to function as a conventional far-field design at the lower frequency. At the lower frequency there would, however, be a shift of the phase center towards the horn aperture, resulting in a phase error in the subreflector illumination and a consequent reduction in efficiency, but perhaps it would be adequate for the intended function. Finally, dual-mode

illumination using the $TE_{11}$ and $TM_{11}$ modes was of interest because of the nearly circular symmetric radiation patterns that can be obtained.[5]

## III. CASSEGRAIN ANTENNA GEOMETRY

Figure 1 shows the geometry of a Cassegrain antenna. It consists of a conical feed horn, a hyperboloid subreflector and a paraboloid main reflector. One focal point of the hyperboloid coincides with the focal point of the paraboloid and the other focal point with the phase center of the horn. The main reflector illumination angle is equal to the geometrical subreflector illumination angle, $\theta_m$. The feed is located in the geometrical shadow region of the subreflector.

The initial design of a Cassegrain antenna is usually based on geometrical optics, which imposes certain restrictions on the antenna geometry. The constraints are that the feed horn be located in the shadow region of the subreflector and that the subreflector intercept most of the power radiated by the horn.

To relate the radiation properties of the horn to the antenna geometry it is convenient to define a parameter $K$ by:

$$K = \frac{d}{\lambda} \sin \delta \tag{1}$$

where

$d$ = horn aperture diameter
$\lambda$ = wavelength
$\delta$ = the angle subtended by the subreflector with respect to the center of the horn aperture (Fig. 1).

For conventional Cassegrain antennas representative values of $K$ are from 1.2 to 1.6. For these values of $K$ the major portion of the main lobe of a narrow angle horn excited by $TE_{11}$ and $TM_{11}$ modes, is intercepted by the subreflector. The lower value of $K$ is preferable for $TE_{11}$ mode excitation because the major lobe of the horn radiation pattern is narrower in the $E$ plane than in the $H$ plane. Beyond the major lobe region the phase variations are too large for efficient subreflector illumination.

For near field Cassegrains the values for $K$ are much larger, such that the radiation characteristics of the horn are primarily determined by the horn flare angle.

For the feed horn to be located in the geometrical shadow region of the subreflector it is necessary that angle $\theta_b$ be not less than angle $\theta_{bh}$,

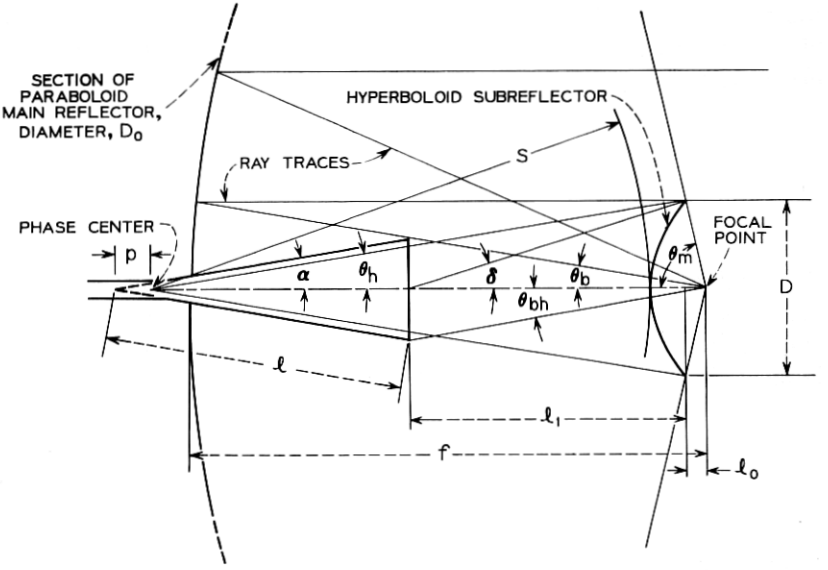


Fig. 1 — Geometry of cassegrain antenna.

that is,

$$\tan \theta_b = B \tan \theta_{bh} \tag{2}$$

where $B$ is a constant with $B \geq 1$. Figure 1 shows the angles $\theta_b$ and $\theta_{bh}$. The horn blocking angle $\theta_{bh}$ can be expressed in terms of the geometrical parameters and (1) by

$$\tan \theta_{bh} = \frac{K\lambda \sin \theta_m}{D \sin (\delta + \theta_m)}. \tag{3}$$

With all other parameters specified, $\theta_{bh}$ is minimum for

$$\delta + \theta_m = \frac{\pi}{2}. \tag{4}$$

Similarly, with $\theta_{bh}$ also specified, $K$ has a maximum value when (4) holds.

Using (2) and (3) and expressing $\theta_b$ in terms of the geometrical parameters, the following equation is obtained for the subreflector diameter, $D$.

$$D = \sqrt{\frac{2BKf\lambda \sin \theta_m}{\sin (\theta_m + \delta) + \dfrac{BK\lambda}{16f} \sin \theta_m}} \tag{5}$$

where

$f$ = focal length of the paraboloid main reflector.

Equation (5) agrees with the previously given condition for no blocking[6] $D \approx (2Kf\lambda)^{1/2}$. In practical antenna designs $BK\lambda/16f$ is small compared with $\sin(\delta + \theta_m)$, hence (5) may be rewritten in terms of the main reflector diameter, $D_o$, as:

$$D \geqq \cos\left(\frac{\theta_m}{2}\right)\sqrt{\frac{K\lambda D_o}{\sin(\delta + \theta_m)}} \tag{6}$$

Equation (6) shows that antennas with large main reflectors also require larger subreflectors, but that the ratio $(D/D_o)^2$ which is a measure of the amount of power blocked by the subreflector is inversely proportional to the main aperture diameter $D_o$. Hence the condition (6) is of importance primarily in the design of relatively small Cassegrain antennas.

Equation (6) also shows, as expected, that a conventional Cassegrain antenna requires a smaller subreflector than a near-field Cassegrain antenna, since $K$ is smaller for the former. However, this disadvantage of the near-field Cassegrain antenna is offset by other advantageous properties.

Another parameter which influences the antenna design is the total Fresnel number of the horn at the subreflector distance, defined by

$$F_t = \frac{d^2}{4\lambda}\left(\frac{1}{l} + \frac{1}{l_1}\right). \tag{7}$$

For a conventional Cassegrain, $F_t$ can be selected, to a certain extent, independently of the antenna geometry, because the radiation properties of the horn are not directly related to the horn length, $l$. For such an antenna with combined $TE_{11}$ and $TM_{11}$ mode excitation, a total Fresnel number in the 0.5-0.65 range would provide a nearly uniform subreflector illumination over a wide frequency range (about 30 per cent) with relatively small phase deviations. For $TE_{11}$ mode excitation, a lower Fresnel number is necessary, because the phase of the $E$-plane horn radiation pattern is more frequency sensitive for larger Fresnel numbers.

For a near field Cassegrain antenna the total Fresnel number is almost directly related to the antenna geometry. Specifically, for an antenna with the horn located in the shadow region of the subreflector

and with a subreflector illumination angle equal to the horn flare angle, $F_t$ is given by

$$F_t = \frac{D}{2\lambda} \frac{\tan \theta_h}{1 - \frac{l_o}{l_1 + l_o}} \tag{8}$$

with

$$\tan \theta_h = \frac{2\frac{D}{4f}}{1 - \left(\frac{D}{4f}\right)^2}. \tag{9}$$

Since $l_o$ is much smaller than $l_1$ the total Fresnel number, $F_t$, is mainly determined by the subreflector diameter $D$.

For a near field Cassegrain it is necessary to have both $K$ and $F_t$ large. Equations (3) and (8) show that these quantities are proportional to $D^2$.

## IV. ANTENNA DIMENSION

For the antenna under consideration the main reflector dimensions were specified. Its diameter, $D_o$ is $224\lambda$ ($\lambda$ = wavelength at the design frequency), its focal length, $f$, is $72.8\lambda$ and the corresponding geometrical illumination angle, $\theta_m$, is 75°.

The initial choice of the other antenna dimensions was based on the following consideration. As shown above, $K$ has a maximum for $\delta + \theta_m = \pi/2$. Using this condition the subreflector diameter, $D$, has been chosen such that the optimum value of $K$ is unity at the lowest frequency ($\lambda_L = 4.5\lambda$). At the design frequency, $K$ is about 3 times larger than is required for a conventional Cassegrain antenna feed. For this value of $K$, $D$ is $25\lambda$. With these parameters a horn with a maximum diameter of $17.6\lambda$ can be located in the shadow region of the subreflectors. The corresponding horn length, $l$, is $100\lambda$. However, a feed horn with these dimensions would introduce, at the lowest frequency, appreciable phase variations at the subreflector owing to the shift of the phase center of the horn radiation pattern. For this reason these horn dimensions were not used in the computations.

The horn dimensions used were $d = 14\lambda$ and $l = 42.5\lambda$. With these horn dimensions $K$ is only slightly less than the optimum value. The location of the phase center, which is $5\lambda$ in the front of the horn vertex, and the subreflector illumination angle, which is less than

the horn flare angle, were chosen on the basis of the computed horn radiation patterns for combined $TE_{11}$ and $TM_{11}$ mode excitations. Table I summarizes the antenna dimensions.

## V. PROGRAM FOR COMPUTING ANTENNA CHARACTERISTICS

Programs have been developed which compute the antenna radiation characteristics and plot the computed radiation patterns. The computational methods are similar to those used in the computation of characteristics of the open Cassegrain antenna.[1] However, only single integrations are used; one integration was eliminated by using the Fresnel region approximation for wide angles and large Fresnel numbers.[2] Appendix A gives the equations used. Appendix B discusses operational aspects of the programs and gives flow diagrams.

The antenna characteristics for combined $TE_{11}$–$TM_{11}$ and $TM_{01}$ mode excitations are computed in one operation. The computer program consists of three parts which compute (*i*) the horn radiation patterns, (*ii*) the subreflector radiation patterns, and (*iii*) the far field radiation patterns.

The horn radiation patterns are computed at a constant radius, $s$, corresponding to the subreflector distance. From these computations the power loss at the subreflector is obtained by integration. The horn radiation patterns are also computed at the subreflector surface to obtain the subreflector illumination.

The subreflector radiation patterns are computed at a constant radius, $f$, and at the main reflector surface. From these computations the power loss at the main reflector and the main reflector illumination is obtained.

From the computed main reflector illumination the aperture gain, aperture efficiency and finally the far field radiation patterns are obtained.

The antenna gain and antenna efficiency are determined from the

TABLE I — ANTENNA DIMENSIONS

| | |
|---|---|
| Main reflector diameter, $D_o$ | 224λ |
| Focal length, $f$ | 72.8λ |
| Main reflector illumination angle, $\theta_m$ | 75° |
| Subreflector diameter, $D$ | 25λ |
| Subreflector illumination angle, $\theta_h$ | 9.5° |
| Horn length, $l$ | 42.5λ |
| Horn flare angle, $\alpha$ | 9.5° |
| Phase center location, $p$ | 5.0λ |

computed aperture gain and efficiency respectively by including the loss at the subreflector and main reflector.

In the computations the phase variations at the sub- and main reflectors are included. Also included is the effect of the main reflector aperture blocking by the subreflector but not the effect of the protruding horn.

An estimate of the antenna noise temperature is obtained by assuming, somewhat arbitrarily, that near the horizon half the power lost at the sub- and main reflectors contributes to noise. At zenith it is assumed that the power lost at the main reflector contributes to noise. A ground temperature of 300°K is used in the computations. The additional noise from possible scattering of the subreflector support and the noise from the wide angle sidelobes of the far field radiation patterns are not included in the computations.

## VI. COMPUTED ANTENNA CHARACTERISTICS

The antenna characteristics have been computed with the above computer program for the following feed horn excitations: (*i*) $TE_{11}$ and $TM_{11}$ at the design frequency, $f_o$, 0.8 $f_o$ and 1.3 $f_o$, and (*ii*) $TE_{11}$ and $TM_{01}$ modes at $f_o$ and 0.22 $f_o$. The antenna characteristics for the different modes and frequencies are summarized in Table II. The tabulated power losses are normalized with respect to the total power radiated by the feed horn.

### 6.1 *$TE_{11}$ and $TM_{11}$ Mode Excitations*

The computations were performed by assuming that the two modes are in phase at the horn aperture. The $TM_{11}$ to $TE_{11}$ power ratio was assumed to be 0.17. This value was used because at the design frequency it minimizes the phase variations of the horn radiation patterns at the subreflector both in the E and H planes.

Computations have been performed at the design frequency, $f_o$, 0.8 $f_o$, and 1.3 $f_o$. This corresponds to about a 50 per cent bandwidth. Except for the expected change in the antenna gain, the antenna radiation characteristics remain virtually the same across this frequency range. This indicates that if a frequency-insensitive conical feed-horn using $TE_{11}$ and $TM_{11}$ mode excitation could be developed, this antenna design is capable of efficient radiation over a 50 per cent bandwidth.

Figures 2 through 6 show the antenna radiation patterns at the design frequency, $f_o$. Included are: the amplitude and phase of the

TABLE II — CALCULATED ANTENNA CHARACTERISTICS

| Frequency | | Design, $f_0$ | | $0.8 f_0$ | $1.3 f_0$ | $f_0$ | $0.222 f_0$ | |
|---|---|---|---|---|---|---|---|---|
| Mode | | $TE_{11}$ and $TM_{11}$ | $TM_{01}$ | $TE_{11}$ and $TM_{11}$ | | $TE_{11}$ | $TE_{11}$ | $TM_{01}$ |
| Per cent of: Power loss at subreflector | | 2.7 | 20.0 | 3.4 | 2.1 | 9.3 | 26.0 | 50.8 |
| Power loss at main reflector | | 0.7 | 2.9 | 0.9 | 0.5 | 1.0 | 4.4 | 5.6 |
| Power blocked by subreflector | | 5.0 | — | 4.8 | 5.5 | 3.3 | 2.9 | — |
| Aperture efficiency | | 72.7 | — | 73.4 | 71.5 | 75.4 | 82.2 | — |
| Antenna efficiency | | 70.4 | — | 70.3 | 69.8 | 67.7 | 57.2 | — |
| Antenna gain, dB | | 55.4 | 49.4 at max | 53.4 | 57.6 | 55.2 | 41.4 | 33.3 at max |
| Antenna noise temperature, °K | Near horizon | 5.1 | 34.35 | 6.45 | 3.9 | 15.45 | 45.6 | 81.6 |
| | At zenith | 2.1 | 8.7 | 2.7 | 1.5 | 3.0 | 13.2 | 16.8 |
| First sidelobe, dB | H plane | −22.7 | −12.9 | −23.9 | −21.4 | −24.1 | −17.2 | −13.9 |
| | E plane | −24.5 | | −23.8 | −24.2 | −15.1 | −21.0 | |

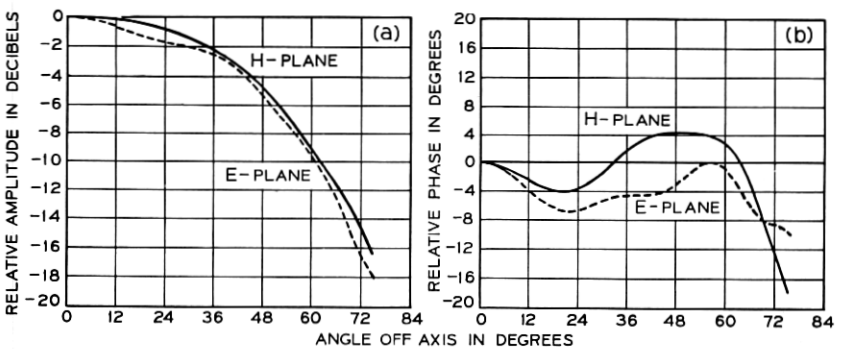


Fig. 2 — Subreflector illumination, $TE_{11}$ and $TM_{11}$ modes, freq. = $f_0$.

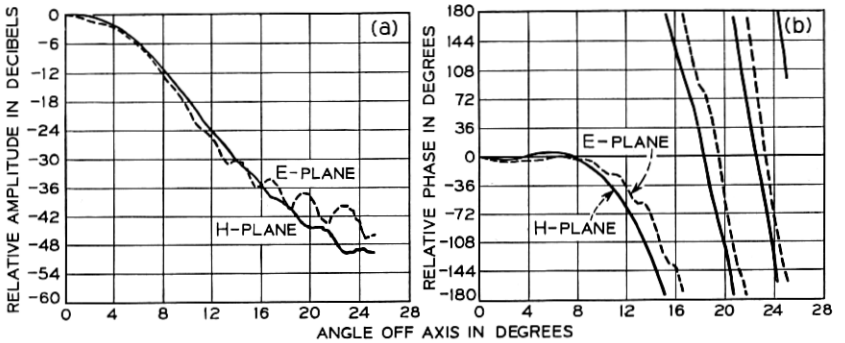


Fig. 3 — Horn radiation pattern at distance S ($TE_{11}$ and $TM_{11}$ modes, freq. $= f_0$)

subreflector illumination, the amplitude and phase of the horn radiation pattern at the subreflector distance, the amplitude and phase of the main reflector illumination, the amplitude and phase of the subreflector radiation pattern at the focal distance, and the far field pattern.

These figures show that the phase variations of the sub- and main reflector illuminations are relatively small at this frequency. This is because the location of the phase center and the ratio of the $TM_{11}$ to $TE_{11}$ modes has been chosen to minimize the phase variations at the subreflector. These figures also show that the far field radiation pattern is virtually the same in the E and H planes. This should result in a nearly circular symmetric far field radiation pattern.

Figures 7 and 8, and Figures 9 and 10 show some of the antenna

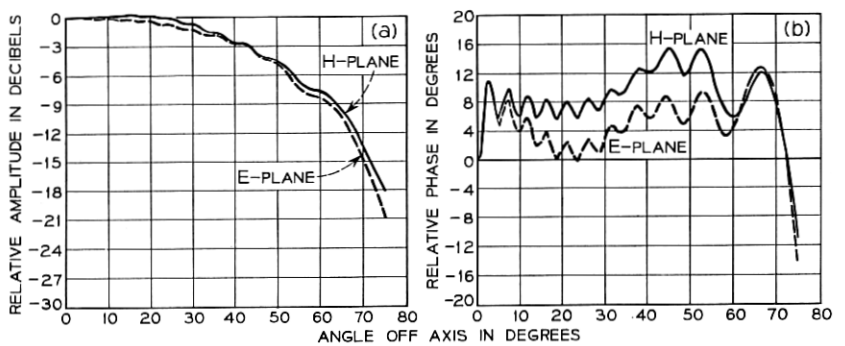


Fig. 4 — Main reflector illumination ($TE_{11}$ and $TM_{11}$ modes, freq. $= f_0$).

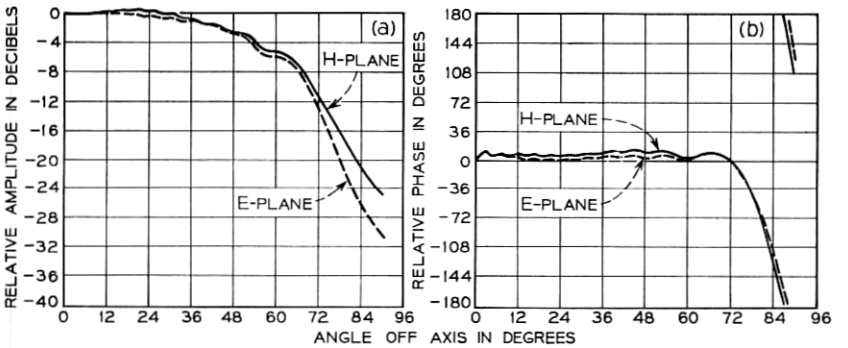


Fig. 5 — Subreflector radiation pattern at focal distance ($TE_{11}$ and $TM_{11}$ modes, freq. = $f_o$).

radiation characteristics at 0.8 $f_o$ and at 1.3 $f_o$, respectively. The phase variations of the sub- and main reflector illuminations, though small, are larger than at the design frequency. This primarily results from the shift in the phase center of the horn radiation pattern. It is the shift in the phase center which ultimately limits the upper frequency of operation for this type of antenna.

### 6.2 *$TM_{01}$ Mode Excitation*

The radiation characteristics for the $TM_{01}$ mode excitation were computed at the design frequency, $f_o$. Figures 11 through 13 show representative radiation patterns for this mode. Particularly pronounced are the amplitude oscillations of the main and subreflector illuminations. This seems to be characteristic for the $TM_{01}$ radiation

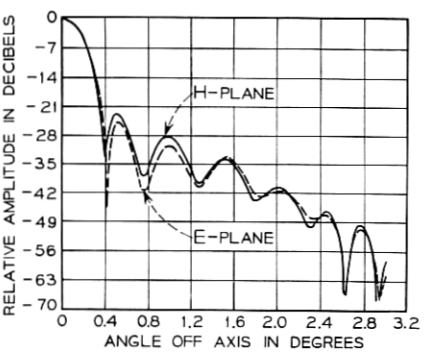


Fig. 6 — Far field radiation pattern ($TE_{11}$ and $TM_{11}$ modes, freq. = $f_o$).

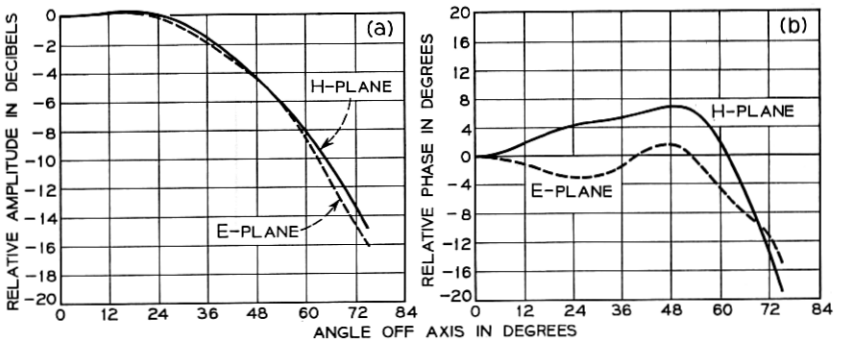


Fig. 7 — Subreflector illumination ($TE_{11}$ and $TM_{11}$ modes, freq. $= 0.80 \times f_0$).

patterns from apertures and reflectors which are large compared with the wavelength and which are illuminated with nearly spherical wave fronts. However, no experimental evidence has been found to confirm these characteristics.

The advantage of this antenna for $TM_{01}$ mode excitation compared with a conventional Cassegrain is less spillover at the subreflector, hence, less antenna noise. However, the sidelobe levels of the far field radiation pattern are perhaps a few dB higher than could be obtained with a conventional Cassegrain.

### 6.3 *$TE_{11}$ Mode Excitation*

In view of the difficulties in realizing a conical feed horn with $TE_{11}$ and $TM_{11}$ mode excitation which would maintain the proper phase

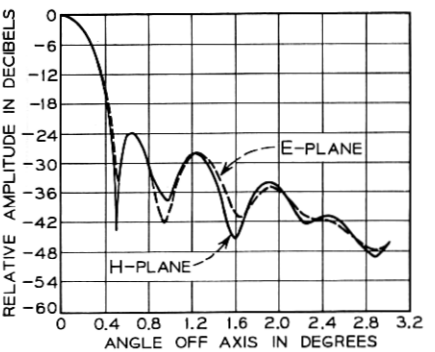


Fig. 8 — Far field radiation pattern ($TE_{11}$ and $TM_{11}$ modes, freq. $= 0.80 \times f_0$).

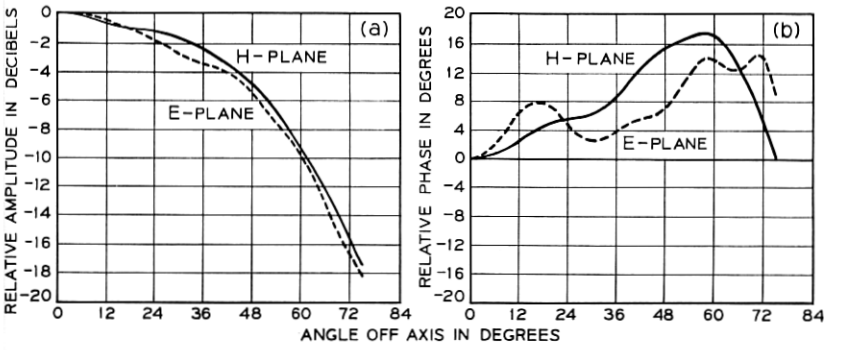


Fig. 9 — Subreflector illumination ($TE_{11}$ and $TM_{11}$ modes, freq. = 1.30 × $f_o$).

relationship at the horn aperture over a wide frequency range, $TE_{11}$ mode excitation only has been investigated for the same antenna geometry.

Figures 14 and 15 show some of the radiation patterns for this mode at the design frequency, $f_o$. The computations show that the phase variations of the sub- and main reflector illuminations are considerably larger, particularly in the E plane, compared with those obtained by using combined $TE_{11}$ and $TM_{11}$ mode excitations. Also, the sidelobe levels of the far field radiation pattern in the E plane are considerably higher than in the H plane.

Table II shows that the computed antenna gain is 0.2 dB lower than the computed gain for $TE_{11}$ and $TM_{11}$ modes. However, the most significant difference is the increase in the antenna noise tem-

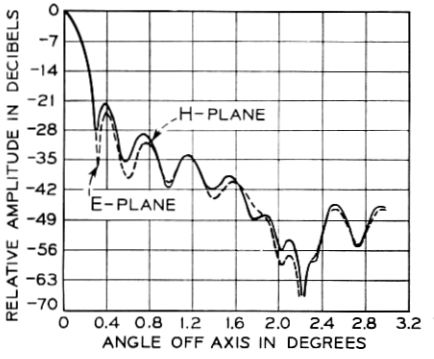


Fig. 10 — Far field radiation pattern ($TE_{11}$ and $TM_{11}$ modes, freq. = 1.30 × $f_o$).

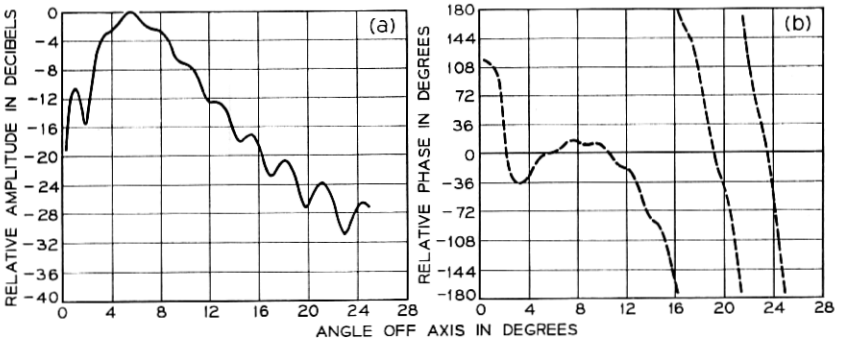


Fig. 11 — Horn radiation pattern at distance S ($TM_{01}$ mode, freq. $= f_0$).

perature by 10°K near the horizon. This increase is primarily caused by the larger power loss at the subreflector because of the E plane horn radiation pattern characteristics.

A reduction of the antenna noise temperature by a few degrees might be possible by increasing the subreflector illumination angle perhaps even beyond the geometrical illumination angle of the horn. Figure 14 shows that the phase variations in the E-plane radiation pattern are not very large in the vicinity of the presently-used subreflector illumination angle of 9.5 degrees. The computed horn power radiation patterns show that if in the present design the illumination angle were 10.5 degrees the antenna noise temperature would be reduced by 4.8°K. The antenna gain for such a design would be reduced by only a small amount.

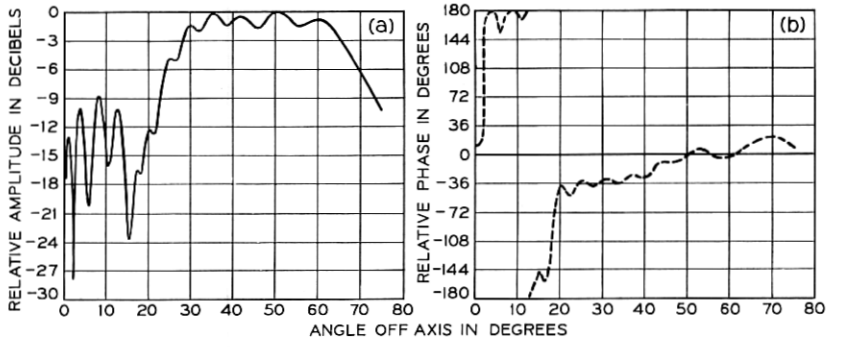


Fig. 12 — Main reflector illumination ($TM_{01}$ mode, freq. $= f_0$).

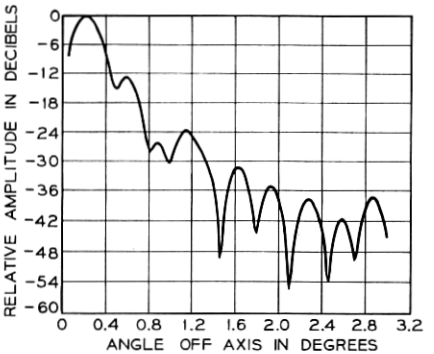


Fig. 13 — Far field radiation pattern ($TM_{01}$ mode, freq. = $f_o$).

The bandwidth characteristics for this mode in the vicinity of the design frequency should be similar to those of the combined $TE_{11}$ and $TM_{11}$ modes.

### 6.4 *$TE_{11}$ and $TM_{01}$ Mode Excitation at* 0.22 $f_o$

The horn and far field radiation patterns for these modes are shown in Figs. 16 through 19. The right side of Table II summarizes the computed antenna performance at 0.22 $f_o$. The antenna efficiency for the $TE_{11}$ mode is relatively high particularly in view of the large phase variations of the subreflector illumination. The far field radiation patterns for both the $TE_{11}$ and $TM_{01}$ modes show good characteristics. The primary disadvantages, however, are the high noise

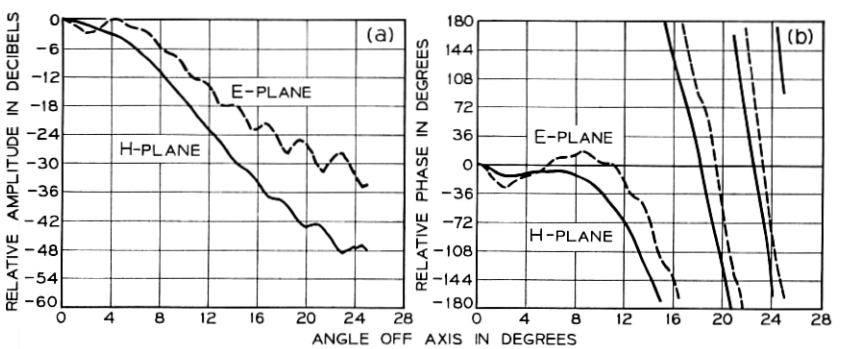


Fig. 14 — Horn radiation pattern at distance S ($TE_{11}$ mode, freq. = $f_o$).

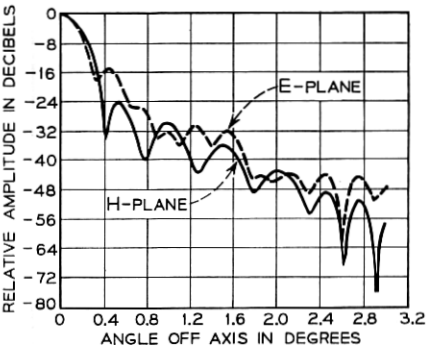


Fig. 15 — Far field radiation pattern ($TE_{11}$ mode, freq. = $f_o$).

temperatures for both modes, owing to the power loss at the subreflector.

## VII. SUMMARY AND CONCLUSIONS

Computer programs have been developed for computing the radiation characteristics of Cassegrain antennas and for plotting of the computed radiation patterns. The method is applicable to symmetrical Cassegrain antennas and provides the means of their design for nearly optimum performance.

A Cassegrain antenna with a near field conical feed horn has been investigated for different mode excitations and over a wide frequency range. For large antennas (over 200 wavelength main reflector diam-

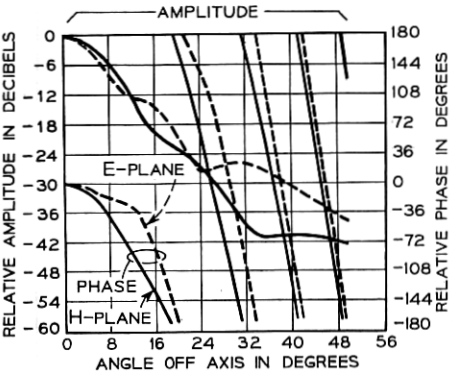


Fig. 16 — Horn radiation pattern at distance S ($TE_{11}$ mode, freq. = $0.22 \times f_o$).

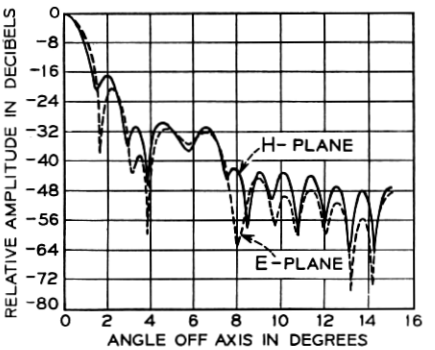


Fig. 17 — Far field radiation pattern ($TE_{11}$ mode, freq. $= 0.22 \times f_o$).

eter) this type of feed can be used over a 50 per cent bandwidth with only small variations in the over-all antenna characteristics, except for the predictable increase in the antenna gain with frequency.

The computed antenna characteristics for the combined $TE_{11}$ and $TM_{11}$ mode excitations show that the advantages of the combined excitation are: (*i*) lower far field E-plane sidelobes, (*ii*) 0.2 dB higher antenna gain, and (*iii*) 10°K lower antenna noise temperature.

At the design frequency for $TE_{11}$ mode excitation, the computed antenna efficiency is 70 per cent and the noise temperature near horizon 15.5°K. With a design modification it should be possible to reduce the noise temperature by a few degrees without affecting the antenna gain.

For the $TM_{01}$ mode, the calculated antenna gain and noise tem-

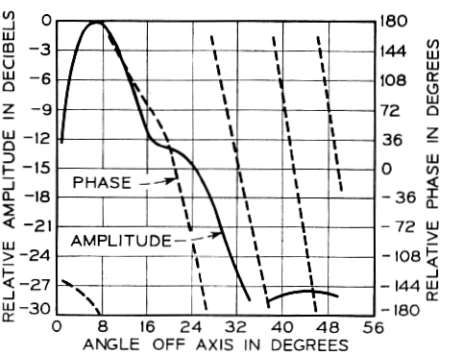


Fig. 18 — Horn radiation pattern at distance S ($TM_{01}$ mode, freq. $= 0.22 \times f_o$).

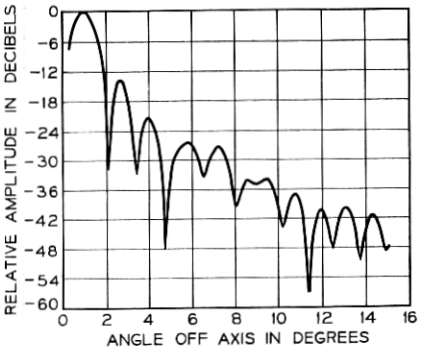


Fig. 19 — Far field radiation pattern ($TE_{11}$ mode, freq. = 0.22 × $f_o$).

perature at the design frequency are superior to those obtainable by using a conventional feed. The sidelobe levels of the far field radiation pattern are perhaps a few dB higher.

At a frequency 4.5 times below the design frequency the calculated antenna efficiencies for the $TE_{11}$ and $TM_{01}$ modes are relatively high. However, the power loss at the subreflector gives rise to appreciable noise temperatures near the horizon.

## APPENDIX A

### *Formulations Used in Computing the Characteristics of Cassegrain Antennas*

#### A.1 *Horn Radiation Patterns*

The horn radiation patterns have been computed by using the Kirchhoff approximation to the aperture radiation field. With this approximation the electric field $\mathbf{E}_p$ at distances of at least a few wavelengths from the aperture is:[7]

$$\mathbf{E}_p = \frac{jk}{4\pi} \iint_S [\mathbf{E}_a(1 + 1_n \cdot 1_R) - \mathbf{E}_a \cdot 1_R(1_n + 1_R)] \frac{e^{-jkR}}{R} ds \qquad (10)$$

where

$S$ = horn aperture area

$k = \frac{2\pi}{\lambda}$

$\lambda$ = wavelength

and $1_n$ and $1_R$ are unit vectors in the normal, and in the $R$ direction as shown in Fig. 20. $\mathbf{E}_a$ is the electric field in the horn aperture, assumed to be the same as for circular waveguide modes but with spherical wave fronts

Since it has been shown by actual computations[4] that the primary contributions to the horn radiation patterns are due to the first terms of (10), in the computations the term $\mathbf{E}\cdot 1_R(1_n + 1_R)$ has been neglected.

Because of the periodicity of the $e^{-ikR}/R$ with respect to the azimuth coordinates $\varphi'$ and $\varphi_1$, it is sufficient to evaluate (10) in a discrete number of $\varphi_1$ planes, the number being equal to number of Fourier components of the aperture field in $\varphi'$. In particular it has been shown[1] that for $TE_{11}$ and $TM_{11}$ mode excitations it is sufficient to evaluate one rectilinear $x$ or $y$ component of (10) in the two principal planes $\varphi_1 = 0$ and $\varphi_1 = \pi/2$. Similarly for $TM_{01}$ mode excitation only one rectilinear component of $\mathbf{E}_a$ in one plane needs to be evaluated.

The integrals which are evaluated for the $TE_{11}$, $TM_{11}$, and $TM_{01}$ modes are:

$$E_{ny} = \frac{kl^2}{4\pi}\int_0^{\alpha}\int_0^{2\pi} E_{ay}\frac{e^{-jkR}}{R}(1 + 1_n\cdot 1_R)\sin\theta'\,d\theta'\,d\varphi' \qquad (11)$$

with the aperture fields for the different modes given by:

*$TE_{11}$ mode*

$$(E_{ay})_{TE_{11}} = J_0\left(k_{TE_{11}}\frac{\theta'}{\alpha}\right) - J_2\left(k_{TE_{11}}\frac{\theta'}{\alpha}\right)\cos 2\varphi' \qquad (12)$$

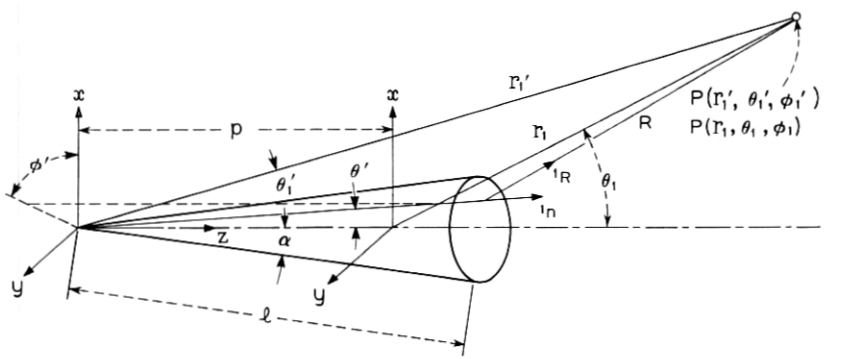


Fig. 20 — Coordinates for horn radiation pattern computation.

with

$$J_1'(k_{TE_{11}}) = 0. \tag{13}$$

*$TM_{11}$ mode*

$$(E_{ay})_{TM_{11}} = J_0\left(k_{TM_{11}} \frac{\theta'}{\alpha}\right) + J_2\left(k_{TM_{11}} \frac{\theta'}{\alpha}\right) \cos 2\varphi' \tag{14}$$

with

$$J_1(k_{TM_{11}}) = 0. \tag{15}$$

*$TM_{01}$ mode*

$$(E_{ay})_{TM_{01}} = J_1\left(k_{TM_{01}} \frac{\theta'}{\alpha}\right) \sin \varphi' \tag{16}$$

with

$$J_0(k_{TM_{01}}) = 0. \tag{17}$$

$J_n$ = Bessel functions of order $n$.

$\alpha$ = horn flare angle.

The integration with respect to $\varphi'$ has been eliminated by approximating the integrals, $I_{nh}$, given by:

$$I_{nh} = \int_0^{2\pi} \frac{e^{-ikR}}{R} (1 + 1_n \cdot 1_R) \cos n(\varphi_1 - \varphi') \, d(\varphi_1 - \varphi'). \tag{18}$$

The approximations used are modifications of the previously derived[2] approximations, $I_n^1$, to the integrals (18) with $1_n \cdot 1_R = 0$. The modifications consist of including the values of $1_n \cdot 1_R$ at the stationary phase points since it has been shown that the previously derived approximations, $I_n^1$, reduce to those obtained by the method of stationary phase, and that $I_n^1$ can be separated into terms which correspond to the stationary phase terms. It is subsequently shown that $R$ can be expressed as:

$$R = r\sqrt{1 - \frac{2u}{r} \cos(\varphi_1 - \varphi')} \tag{19}$$

where $r$ and $u$ are functions which are independent of $\varphi$ and $\varphi'$, on this basis, the first order approximations to (18), $I_{nh}^1$ are:

$$I^1_{nh} = \pi j^n \left\{ \left[ \frac{e^{-jk(R_o+u)}}{R_o} (1 + 1_n \cdot 1_{R_o}) + \frac{e^{-jk(R_1-u)}}{R_1} (1 + 1_n \cdot 1_{R_1}) \right] J_n(ku) \right.$$
$$\left. - j \left[ \frac{e^{-jk(R_o+u)}}{R_o} (1 + 1_n \cdot 1_{R_o}) - \frac{e^{-jk(R_1-u)}}{R_1} (1 + 1_n \cdot 1_{R_1}) \right] J'_n(ku) \right\} \quad (20)$$

with

$$R_o = r\left(1 - \frac{2u}{r}\right)^{\frac{1}{2}} \quad (21)$$

$$R_1 = r\left(1 + \frac{2u}{r}\right)^{\frac{1}{2}} \quad (22)$$

and $1_{R_o}$ and $1_{R_1}$ are the unit vectors at $(\varphi_1 - \varphi')$ equal to zero and $\pi$ respectively.

By using the approximation (20), one integration is eliminated in (11) and the radiation patterns for the different modes are computed from the following integrals:

*$TE_{11}$ Mode*

$$(E_{p\psi})_{TE_{11}} = \frac{jkl^2}{4\pi} \int_0^\alpha \left[ J_o\left(k_{TE_{11}} \frac{\theta'}{\alpha}\right) I^1_{oh} \pm J_2\left(k_{TE_{11}} \frac{\theta'}{\alpha}\right) I^1_{2h} \right] \sin \theta' \, d\theta' \quad (23)$$

where the minus signs give the radiation pattern in the plane $\varphi_1 = 0$ and the plus sign the radiation pattern in the plane $\varphi_1 = \pi/2$.

*$TM_{11}$ mode*

The integral is analogous to (23).

*$TM_{01}$ mode*

$$(E_{p\psi})_{TM_{01}} = \frac{jkl^2}{4\pi} \int_0^\alpha J_1\left(k_{TM_{01}} \frac{\theta'}{\alpha}\right) I^1_{1h} \sin \theta' \, d\theta'. \quad (24)$$

Referring to Fig. 20,

$$R = (l^2 + r_1^2 + p^2 + 2r_1 p \cos \theta_1 - 2lp \cos \theta' - 2r_1 l \cos \gamma_1)^{\frac{1}{2}} \quad (25)$$

with

$$\cos \gamma_1 = \sin \theta_1 \sin \theta' \cos (\varphi' - \varphi_1) + \cos \theta_1 \cos \theta' \quad (26)$$

and

$$1_n \cdot 1_R = \frac{p \cos \theta' - l + r_1 \cos \gamma_1}{R}. \quad (27)$$

Hence a comparison of (25) with (19) shows that

$$r = (l^2 + r_1^2 + p^2 + 2r_1 p \cos\theta_1 - 2lp \cos\theta' - 2r_1 l \cos\theta_1 \cos\theta')^{\frac{1}{2}} \quad (28)$$

and

$$u = \frac{r_1 l \sin\theta_1 \sin\theta'}{r}. \quad (29)$$

The integrals for the difference modes have been computed at two values of $r_1$: (*i*) at the subreflector surface to obtain the subreflector illumination, and (*ii*) at a constant distance corresponding to shortest distance, $s$, from the subreflector to the horn aperture. The latter was performed to obtain the horn radiation pattern in a form which is readily measurable and convenient for subsequent computation of the horn power radiation pattern used for determining the power loss at the subreflector.

For the first computation referring to Fig. 21

$$r_1 = \frac{c}{2} \frac{(1 - \beta^2)}{\cos\theta_1 - \beta} \quad (30)$$

with

$$\beta = \frac{b}{c}.$$

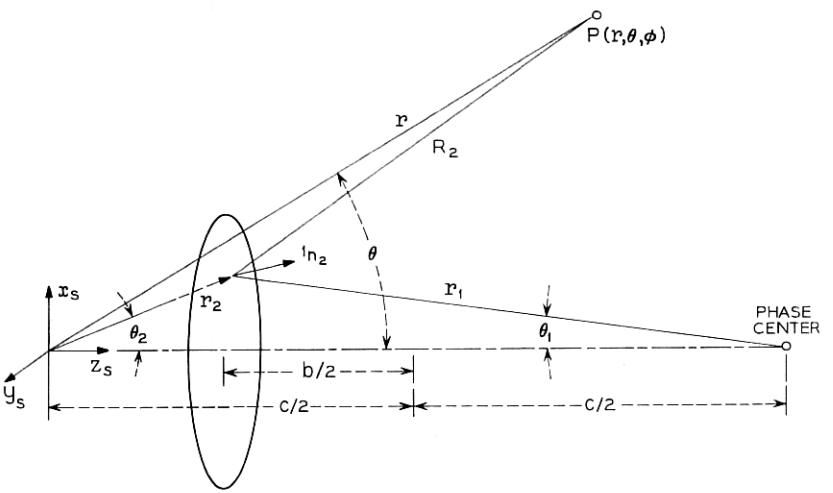


Fig. 21 — Subreflector coordinates.

For determining the subreflector illumination it is preferable to obtain the illumination in terms of subreflector coordinate $\theta_2$. The relationship between the coordinates $\theta_1$ and $\theta_2$ is:

$$\cos \theta_1 = \frac{(1 + \beta^2) \cos \theta_2 + 2\beta}{1 + \beta^2 + 2\beta \cos \theta_2}. \tag{31}$$

The second computation

$$r_1 = \frac{c}{2}(1 + \beta) \tag{32}$$

and the integration is performed as a function of $\theta_1$.

A comparison has been made between some radiation patterns computed by single and double integration. Good agreement was obtained.

The electric field in the spherical $\theta_1$ and $\varphi_1$ coordinates can be expressed in terms of the radiation patterns in the principal planes $\varphi_1 = 0, \pi/2$.

For $TE_{11}$ and $TM_{11}$ modes

$$\mathbf{E}_p = 1_{\theta_1} E_{p\nu}\left(\frac{\pi}{2}\right) \sin \varphi_1 + 1_{\varphi_1} E_{p\nu}(0) \cos \varphi_1 \tag{33}$$

The $TM_{01}$ mode has only a $\theta_1$ component given by (24).

A.2 *Horn Power Radiation Patterns*

The horn power radiation pattern, $P_H$, is computed from the following integral:

$$P_H = \frac{r_1^2}{2\eta} \int_0^{2\pi} \int_0^{\theta_1} \mathbf{E}_p \cdot \mathbf{E}_p^* \sin \theta \, d\theta \, d\varphi. \tag{34}$$

$\eta$ = free space intrinsic impedance.

The total power is obtained by extending the range of $\theta_1$ to the region where $\mathbf{E}_p \cdot \mathbf{E}_p^*$ has a negligible value.

The total radiated power can also be obtained from the assumed fields at the aperture (12) through (17). On this basis the total power for the different modes is approximately

*$TE_{11}$ mode*

$$P_{H_t} = \frac{2\pi(l\alpha)^2}{2\eta} [k_{\mathrm{TE}_{11}}^2 - 1]\left[\frac{J_1(k_{TE_{11}})}{k_{\mathrm{TE}_{11}}}\right]^2. \tag{35}$$

*$TM_{11}$ mode*

$$P_{H_t} = \frac{2\pi(l\alpha)^2}{2\eta} J_0^2(k_{\mathrm{TM}_{11}}). \tag{36}$$

*$TM_{01}$ mode*

$$P_{H_1} = \frac{\pi(l\alpha)^2}{2\eta} J_1^2(k_{\mathrm{TM}_{01}}) \cdot \tag{37}$$

The computations performed for the different modes and frequencies by using (34) are in agreement with (35) through (37) within 1.8 per cent, with the power computed by using (34) giving larger values for all modes. This is at least partially caused by the higher values that the approximations $I_n^1$ give compared with those obtained by precise numerical integration.[2]

A.3 *Subreflector Radiation Patterns*

The subreflector radiation patterns have been computed by using the surface integral relating the radiated fields and the current distribution over a surface.[7] For the distance of at least a few wavelengths from the reflector the radiated electric field with reference to Fig. 21 is:

$$E_s = \frac{j}{\lambda} \iint_{S_s} 1_{R_2} \times (\mathbf{J} \times 1_{R_2}) \frac{e^{-jk(R_2 + r_2)}}{R_2} ds_2 \tag{38}$$

where

$\mathbf{J}$ = surface current density
$S_s$ = subreflector area.

To evaluate (38) it has been assumed that the reflector is locally plane. With this assumption the current density is directly related to the incident electric field. To simplify the computations $1_{R_2}$ was replaced by $1_{r_2}$. (A test computation of the subreflector radiation pattern of the open Cassegrain antenna showed that using $1_{r_2}$ instead of $1_{R_2}$ results in a negligible difference.)

For a hyperboloid reflector, the relations between the incident electric field and the current density have been derived.[1] By using the approximation (20) the integration with respect to $\varphi_2$ can be eliminated. On this basis the radiated fields of the subreflector resulting from the incident fields of a $\mathrm{TE}_{11}$ mode (23), are given by:

In the plane $\varphi_2 = 0$,

$$[E_s(0)]_{\mathrm{TE}_{11}} = -\frac{j}{2\lambda} \int_0^{\theta_m} e^{-jkr_2} \left\{ \left[ E_{pv}(0) + E_{pv}\left(\frac{\pi}{2}\right) \frac{(1 + \beta \cos\theta_2)}{(\beta + \cos\theta_2)} \right] I_o^1 + \left[ E_{pv}(0) - E_{pv}\left(\frac{\pi}{2}\right) \frac{(1 + \beta \cos\theta_2)}{\beta + \cos\theta_2} \right] I_2^1 \right\} r_2^2 \sin\theta_2 \, d\theta_2 \, . \tag{39}$$

In the plane $\varphi_2 = \pi/2$,

$$\left[E_s\left(\frac{\pi}{2}\right)\right]_{\mathrm{TE}_{11}}$$

$$= -\frac{j}{2\lambda}\int_0^{\theta_m} e^{-jkr_2}\left\{\left[E_{py}(0) + E_{py}\left(\frac{\pi}{2}\right)\frac{(1+\beta\cos\theta_2)}{\beta+\cos\theta_2}\right]I_o^1\cos\theta\right.$$

$$-\left[E_{py}(0) - E_{py}\left(\frac{\pi}{2}\right)\frac{(1+\beta\cos\theta_2)}{\beta+\cos\theta_2}\right]I_2^1\cos\theta$$

$$\left.+\,2E_{py}\left(\frac{\pi}{2}\right)\frac{\sin\theta_2}{\beta+\cos\theta_2}I_1^1\sin\theta\right\}r_2^2\sin\theta_2\,d\theta_2\,. \tag{40}$$

For the $\mathrm{TM}_{11}$ mode, the fields are analogous to (39) and (40) with the corresponding $\mathrm{TM}_{11}$ illuminated functions $E_p(0)$ and $E_p(\pi/2)$.

For the $\mathrm{TM}_{01}$ mode,

$$[E_s(0)]_{\mathrm{TM}_{01}} = -\frac{j}{2\lambda}\int_0^{\theta_m} E_{py}(0)\,e^{-jkr_2}$$

$$\cdot\left[\cos\theta\,\frac{(1+\beta\cos\theta_2)}{\beta+\cos\theta_2}I_1^1 + \frac{\beta\sin\theta\sin\theta_2}{\beta+\cos\theta_2}I_o^1\right]r_2^2\sin\theta_2\,d\theta_2 \tag{41}$$

where $E_p(0)$ is given by (24).

In the above $r_2$ is the equation of the subreflector in the coordinates shown in Fig. 21, and is given by

$$r_2 = \frac{c}{2}\frac{(1-\beta^2)}{\beta+\cos\theta_2}. \tag{42}$$

$I_n^1$ are the first order approximations to the integration with respect to $\varphi_2$. They are given by (20) with $1_n \cdot 1_{R_o}$ and $1_n \cdot 1_{R_1}$ set equal to zero. The other parameters are:

$$R_2 = (r^2 + r_2^2 - 2rr_2\cos\gamma_2)^{\frac{1}{2}}. \tag{43}$$

$$\cos\gamma_2 = \sin\theta\sin\theta_2\cos(\varphi-\varphi_2) + \cos\theta\cos\theta_2\,. \tag{44}$$

$$u_2 = \frac{rr_2\sin\theta\sin\theta_2}{(r^2+r_2^2-2rr_2\cos\theta\cos\theta_2)^{\frac{1}{2}}}. \tag{45}$$

The subreflector radiation patterns have been computed at two distances: at the paraboloid surface

$$r = \frac{2f}{1+\cos\theta} \tag{46}$$

where $f$ = focal length of the main reflector, to obtain the main reflector illumination, and at

$$r = f \tag{47}$$

to determine the power loss at the main reflector.

The $\varphi$ dependence of the subreflector radiation patterns are obtained in terms of radiation patterns in the principal planes and are:

*For $TE_{11}$ or $TM_{11}$ modes*

$$[\mathbf{E}_s]_{TE_{11},TM_{11}} = 1_\varphi E_s(0) \cos\varphi + 1_\theta E_s\left(\frac{\pi}{2}\right) \sin\varphi. \tag{48}$$

*For the $TM_{01}$ mode*

$$[\mathbf{E}_s]_{TM_{01}} = 1_\theta E_s(0). \tag{49}$$

The power radiation pattern of the subreflector is computed by using the integral (34).

A.4 *Aperture Gain and Efficiency*

The aperture gain and efficiency are computed by projecting the incident field on the main reflector aperture. The fields in the rectilinear $x$, $y$ components are related to $\theta$, $\varphi$ components by the expressions

$$E_{rs} = -1_x(E_{s\theta} \cos\varphi - E_{s\varphi} \cos\varphi) - 1_y(E_{s\theta} \sin\varphi_2 + E_{s\varphi} \cos\varphi_2). \tag{50}$$

For $TE_{11}$ and $TM_{11}$ mode excitations polarized in the $y$ direction, the gain on axis, $G_M$, is

$$G_M = \frac{4\pi^2}{\lambda^2} \frac{\left| \int_{\theta_b}^{\theta_m} \left[ E_s\left(\frac{\pi}{2}\right) + E_s(0) \right] r^2 \sin\theta \, d\theta \right|^2}{\int_0^{\theta_m} \left[ \left| E_s\left(\frac{\pi}{2}\right) \right|^2 + |E_s(0)|^2 \right] r^2 \sin\theta \, d\theta} \tag{51}$$

where $r$ is the equation for the paraboloid (46).

The aperture efficiency, $g$, is obtained from the relation

$$g = \frac{G}{G_o} \tag{52}$$

with

$$G_o = \left[ \frac{4\pi f \sin\theta_m}{\lambda(1 + \cos\theta_m)} \right]^2. \tag{53}$$

The maximum antenna gain for the $TM_{01}$ mode is determined by normalizing the amplitude of the $TM_{01}$ mode electric field at the horn aperture with respect to the amplitudes of the $TE_{11}$ or $TE_{11}$ and $TM_{11}$ modes for the same power input, by using (35 through 37). The gain for the $TM_{01}$ mode is then related to the gain for the $TE_{11}$ mode on axis, referred to the maximum of its pattern.

A.5 *Far Field Radiation Patterns*

The far field patterns are computed from the projected field on the aperture, using the relation

$$\mathbf{E}_f = \frac{j}{\lambda}\frac{e^{-jkr_a}}{r_a} \cdot \int_{\theta_b}^{\theta_m}\int_0^{2\pi} \mathbf{E}_{rs} \exp\left[jkr \sin\theta \sin\theta_a \cos(\varphi - \varphi_a)\right] r^2 \sin\theta \, d\theta \, d\varphi \qquad (54)$$

where $r_a$, $\theta_a$, and $\varphi_a$ are the coordinates of the far field observation point.

Because of the antenna symmetry the integration with respect to $\varphi$ can be the readily performed. The resulting integration with respect to $\theta$ is for $TE_{11}$ or $TM_{11}$ modes

$$(E_{fy})_{TE_{11}} = -\frac{j\pi}{\lambda}\frac{e^{-jkr_a}}{r_a}\int_{\theta_b}^{\theta_m}\left\{\left[E_s(0) + E_s\left(\frac{\pi}{2}\right)\right]J_0\left(\frac{2\pi r}{\lambda}\sin\theta\sin\theta_a\right) \pm \left[E_s\left(\frac{\pi}{2}\right) - E_s(0)\right]J_2\left(\frac{2\pi r}{\lambda}\sin\theta\sin\theta_a\right)\right\} r^2 \sin\theta \, d\theta \qquad (55)$$

where $\pm$ signs correspond to the patterns in the $H(\varphi_a = 0)$ or $E(\varphi_a = \pi/2)$ planes.

Similarly for the $TM_{01}$ mode

$$(\mathbf{E}_f)_{TM_{01}} = 1_{\theta_a}\frac{2\pi}{\lambda}\frac{e^{-jkr_a}}{r_a}\int_{\theta_b}^{\theta_m} E_s(0) J_1\left(\frac{2\pi r}{\lambda}\sin\theta\sin\theta_a\right) r^2 \sin\theta \, d\theta \qquad (56)$$

where $E_s$ is the main reflector illumination (48) and (49) for the different modes in the planes $\varphi = 0$ and $\varphi = \pi/2$.

## APPENDIX B

*Program for Computing the Characteristics of Cassegrain Antennas and for Graphic Display of Radiation Fields*

The package consists of two programs: a program to compute the horn radiation patterns, the subreflector radiation patterns, the far field radiation patterns, and other characteristics of Cassegrain antennas described in Appendix A, and a program to scale, label, and plot the radiation fields. The two programs are linked by intermediate storage of computed results and control variables on tape, at the conclusion of Part 1 execution.

B.1 *Computation Program*

Figure 22 is a logic diagram of the program. The following convention is used throughout the logic diagram. Square-bracketed symbols

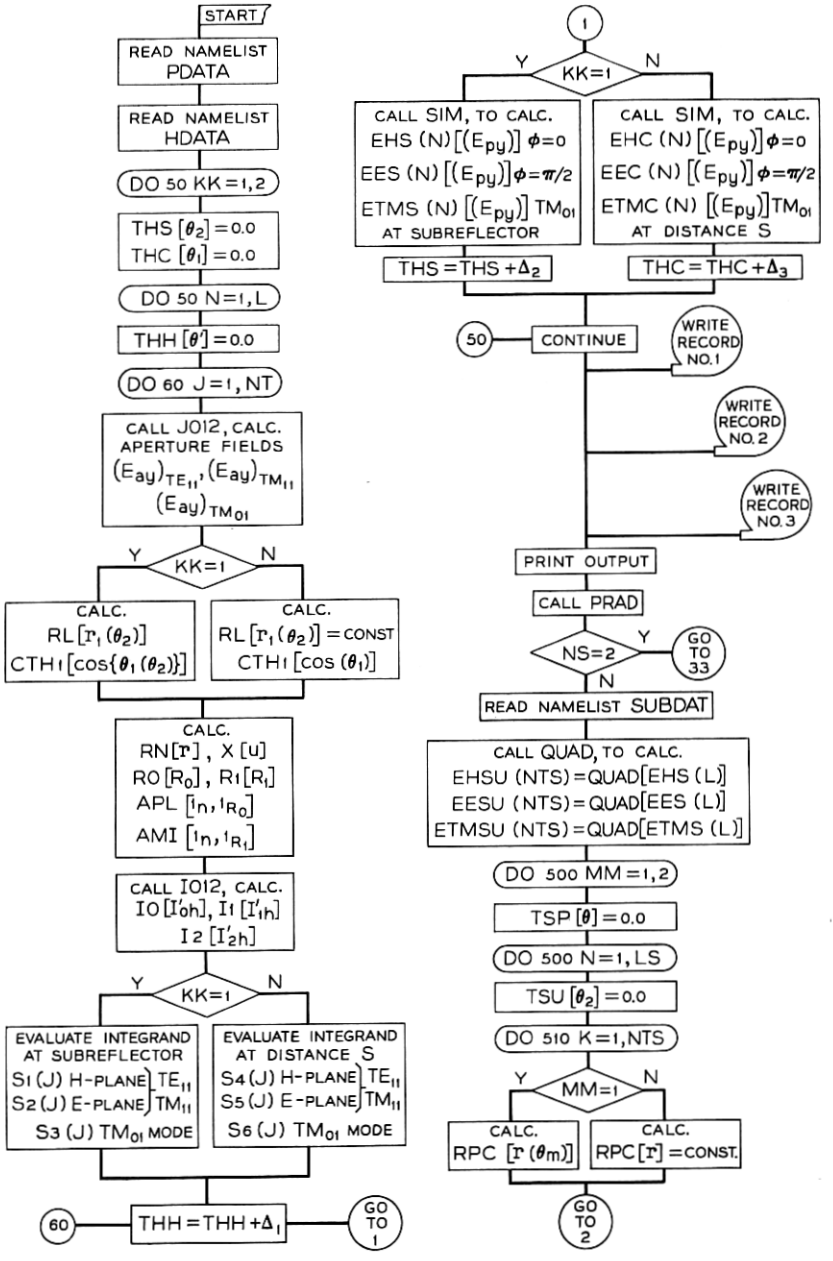
START
READ NAMELIST PDATA
READ NAMELIST HDATA
DO 50 KK=1,2
THS [θ2] =0.0
THC [θ1] =0.0
DO 50 N=1,L
THH [θ'] =0.0
DO 60 J=1,NT
CALL J012, CALC. APERTURE FIELDS (Eay)TE11, (Eay)TM11 (Eay)TM01
Y KK=1 N
CALC. RL [r1 (θ2)] CTH1 [cos{θ1 (θ2)}]
CALC. RL [r1 (θ2)] =CONST CTH1 [cos (θ1)]
CALC. RN [r], X [u] R0 [R0], R1 [R1] APL [1n, 1R0] AMI [1n, 1R1]
CALL I012, CALC. I0 [I'0h], I1 [I'1h] I2 [I'2h]
Y KK=1 N
EVALUATE INTEGRAND AT SUBREFLECTOR S1 (J) H-PLANE TE11 S2 (J) E-PLANE TM11 S3 (J) TM01 MODE
EVALUATE INTEGRAND AT DISTANCE S S4 (J) H-PLANE TE11 S5 (J) E-PLANE TM11 S6 (J) TM01 MODE
60 THH=THH+Δ1 GO TO 1
1
Y KK=1 N
CALL SIM, TO CALC. EHS (N) [(Epy)] φ=0 EES (N) [(Epy)] φ=π/2 ETMS (N) [(Epy)] TM01 AT SUBREFLECTOR
CALL SIM, TO CALC. EHC (N) [(Epy)] φ=0 EEC (N) [(Epy)] φ=π/2 ETMC (N) [(Epy)] TM01 AT DISTANCE S
THS=THS+Δ2
THC=THC+Δ3
50 CONTINUE
WRITE RECORD NO. 1
WRITE RECORD NO. 2
WRITE RECORD NO. 3
PRINT OUTPUT
CALL PRAD
NS=2 Y GO TO 33
N
READ NAMELIST SUBDAT
CALL QUAD, TO CALC. EHSU (NTS) =QUAD [EHS (L)] EESU (NTS) =QUAD [EES (L)] ETMSU (NTS) =QUAD [ETMS (L)]
DO 500 MM=1,2
TSP [θ] =0.0
DO 500 N=1,LS
TSU [θ2] =0.0
DO 510 K=1,NTS
Y MM=1 N
CALC. RPC [r (θm)]
CALC. RPC [r] =CONST.
GO TO 2

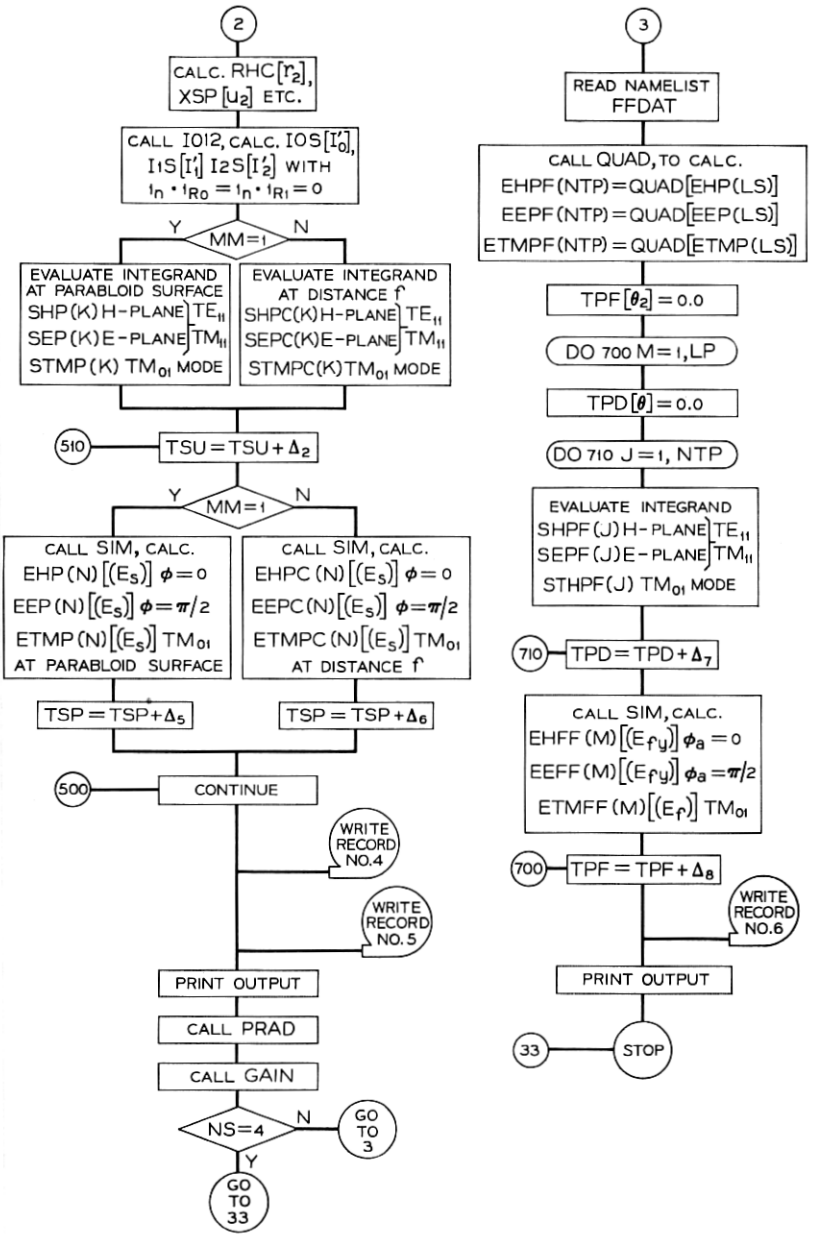


Fig. 22 — Logic diagram for field calculation program.

follow the notation of Appendix A, while the preceding alphanumeric symbols are the Fortran IV source program names.

Four groups of input data are required, designated by the NAMELIST names PDATA, HDATA, SUBDAT, and FFDAT. Although some of the following data is redundant, the formats are designed for convenience and precaution.

**PDATA**

NS — Number of sets of field patterns to be computed, that is,

NS = 2 Horn radiation patterns only
NS = 4 Horn and subreflector patterns
NS = 5 The above plus far field patterns

NPS — Number of patterns per set, that is,

NPS = 2 E & H planes only
NPS = 3 The above plus $TM_{01}$ mode

ITE — Control bit for plotting program (see Section 2)

**HDATA**

HL — Horn length
HLAMD — Horn length normalized with respect to design wavelength
FQ — Frequency normalized with respect to design frequency
C — Distance between foci of hyperboloid
BETA — Defined by equation (30)
PL — Location of phase center normalized with respect to horn length
ALPHA — Horn flare angle
L — Number of points at which horn radiation pattern will be evaluated
NT — Number of points at which integrand will be calculated for evaluation of integrals in equations (23) and (24).
DEG — Angular increment (in degrees) for obtaining subreflector illumination
ANG — Angular increment (in degrees) for obtaining horn radiation patterns
$TM_{11}$ — Complex constant which determines $TM_{11}$ mode to $TE_{11}$ mode ratio
I1P — Control bit for plotting program (See Section B.2.)

**SUBDAT**

F — Focal length of paraboloid
Note: The dimensional unit for F, C, HL must be the same.
FLAMD — Focal length normalized with respect to design wavelength
CLAMD — $C$ normalized with respect to design wavelength
LS — Number of points at which subreflector radiation pattern will be evaluated
NTS — Number of points at which integrand will be calculated for evaluation of integrals in equations (39), (40), and (41)
GAMA — Main reflector illumination angle (degrees)
DEGP — Angular increment (in degrees) for obtaining main reflector illumination
ANGP — Angular increment (in degrees) for obtaining subreflector radiation patterns
INCS — $(N + 1)$ where $N$ is the number of points to be interpolated between previously computed subreflector illumination points
LB — Number of points which are not included in integral (51) because of subreflector blocking
I2P — Control bit for plotting program (See Section B.2.)

**FFDAT**

NTP — Number of points at which integrand will be calculated for evaluation of integrals in equations (55) and (56)
GAMAB — Angular portion (in degrees) of main reflector blocked by subreflector
NTPB — Number of points which are not included in integrals in equations (55) or (56) owing to subreflector blocking after interpolation of main reflector illumination
LP — Number of points at which far field radiation patterns will be evaluated
INCP — $(N + 1)$ where $N$ is the number of points to be interpolated between previously computed main reflector illumination points
DEGFF — Angular increment (in degrees) at which far field radiation pattern will be evaluated
I3P — Control bit for plotting program (See Section B.2.)

The following subprograms must be included in the deck before execution.

PRAD — Computes the power radiation patterns in accordance with equation (34)

JO12 — A Bessel function subroutine developed by J. Alan Cochran and P. A. Alsberg. The present version includes two subsidiary subroutines:[8]

DPHASE — Uses phase-amplitude method for large values of argument

JLOW — Uses downward recursion technique for small values of argument

IO12 — Calculates the first order approximations $I^1_{nh}$ (20) to the integrals $I_{nh}$ (18)

QUAD — A quadratic interpolation scheme for complex arrays

INTERP — A subroutine called by QUAD

PROC — A subroutine to format and print output data

SIM — A complex Simpson's rule integration routine. Will accept an even or odd length array with negligible variation in accuracy

GAIN — Computes the antenna gain and aperture efficiency as defined by equations (51), (52), and (53)

TR — A special purpose of Simpson's rule integration to evaluate the integrals in equation (51). This function subprogram is called only by the GAIN subroutine

The program requires approximately $(52{,}660)_8$ or $(22{,}000)_{10}$ words of storage. A representative execution time for both modes ($TE_{11}$ and $TM_{11}$ combined, and $TM_{01}$) at the design frequency is 14 minutes; the same calculations at 0.22 times the design frequency, where a smaller number of integration points is required, takes approximately 5 minutes.

### B.2 *Plotting Program*

A logic diagram of the program is presented in Fig. 23.

All input data required by the plotting program has been stored on tape by the previous program.

The plotting control bits, referred to in Section 1, have the following meaning: if field calculations are to be made in a combined $TE_{11}$ and $TM_{11}$ mode—that is, input data $TM_{11} \neq (0.0, 0.0)$—the control bit ITE in NAMELIST PDATA must be set equal to 2. If the field calculations are to be made in the $TE_{11}$ mode alone—that is, $TM_{11} = (0.0, 0.0)$—the control bit should be set equal to 1. Therefore calcu-

lations for the three sets of radiation patterns, horn, subreflector, and far field, will generally be made in two modes, a combined $TE_{11}$ and $TM_{11}$ mode, and the $TM_{01}$ mode, where it is understood that the combined mode may be the pure $TE_{11}$ mode, if $TM_{11} = (0.0, 0.0)$ and ITE = 1.

For the combined mode the radiation fields will be evaluated in both E and H planes. E- and H-plane data are plotted together for ease of comparison. However, in some cases (particularly for certain far field patterns) a rapidly varying phase plot superimposed on a rapidly varying amplitude plot may result in an unclear graph. For this reason the control bits I1P, I2P, and I3P are introduced. I1P controls horn radiation pattern plotting, I2P controls subreflector plotting, and I3P, far field plotting. If the control bit for a particular field is set equal to 0, two plots will be generated, that is,

*Combined Mode*

(*i*) E-plane and H-plane amplitude and phase

*$TM_{01}$ Mode*

(*ii*) Phase and amplitude

However, if the control bit is set equal to 1, four plots will be generated:

*Combined Mode*

(*i*) E-plane amplitude and H-plane amplitude
(*ii*) E-plane phase and H-plane phase

*$TM_{01}$ Mode*

(*iii*) Amplitude
(*iv*) Phase

Vertical scales are restricted to allow only 20 divisions, therefore a preferred set of increments for the various scales has been selected. The allowed increments in dB for the amplitude scale, stored in array ADB(I), are:

0.5, 1.0, 1.5, 2.0, 2.5, 3.0, 4.0;

for the phase scale, in degrees in array APH(I):

1.0, 2.0, 3.0, 4.0, 5.0, 6.0, 8.0, 10.0, 12.0, 15.0, 18.0;

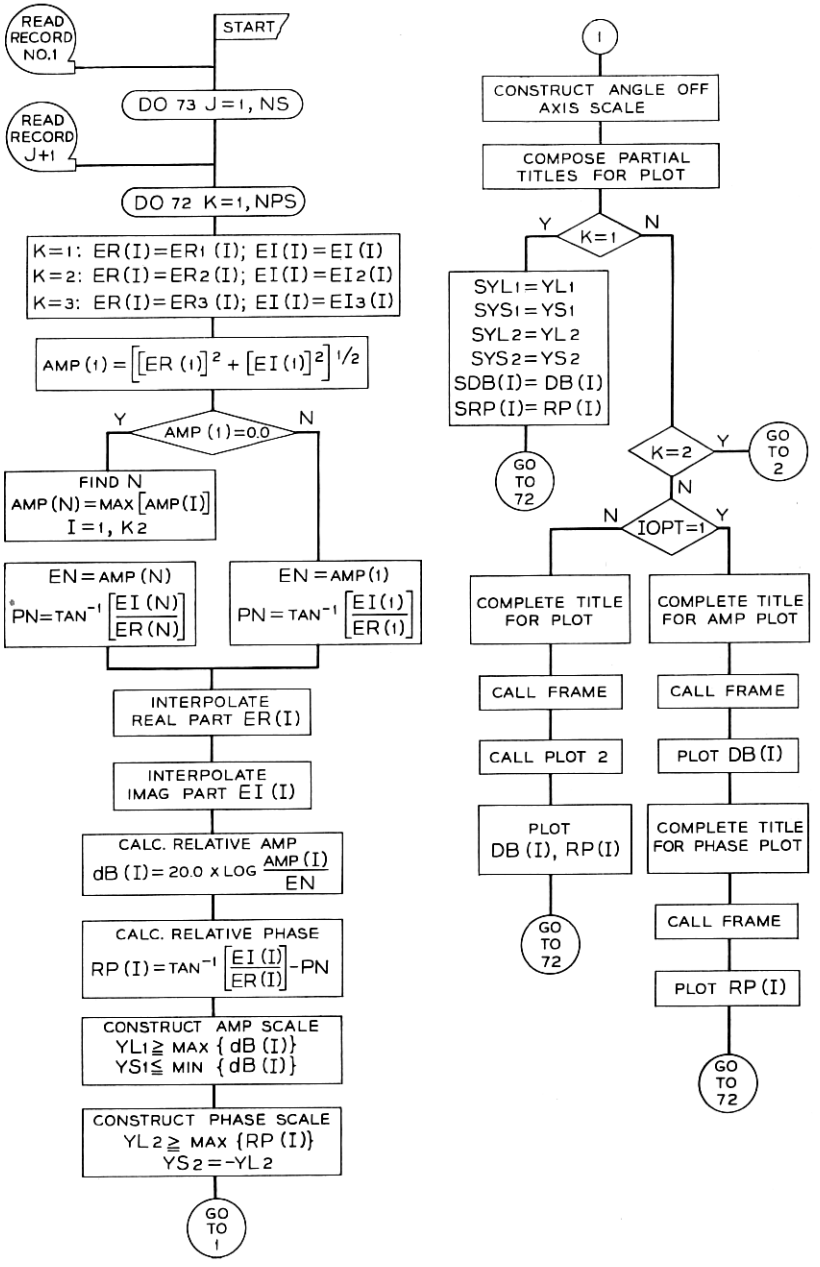
READ RECORD NO.1
START
DO 73 J=1, NS
READ RECORD J+1
DO 72 K=1, NPS
K=1: ER(I)=ER1 (I); EI(I)=EI(I)
K=2: ER(I)=ER2(I); EI(I)=EI2(I)
K=3: ER(I)=ER3(I); EI(I)=EI3(I)
AMP(1) = [[ER (1)]² + [EI (1)]²]^1/2
Y
AMP (1)=0.0
N
FIND N
AMP(N) = MAX [AMP(I)]
I=1, K2
EN = AMP (N)
PN=TAN⁻¹ [EI (N) / ER(N)]
EN = AMP(1)
PN = TAN⁻¹ [EI(1) / ER(1)]
INTERPOLATE REAL PART ER(I)
INTERPOLATE IMAG PART EI (I)
CALC. RELATIVE AMP
dB (I) = 20.0 x LOG AMP (I) / EN
CALC. RELATIVE PHASE
RP (I) = TAN⁻¹ [EI (I) / ER (I)] - PN
CONSTRUCT AMP SCALE
YL1 ≧ MAX { dB (I)}
YS1 ≦ MIN {dB (I)}
CONSTRUCT PHASE SCALE
YL2 ≧ MAX {RP (I)}
YS2 = -YL2
GO TO 1
1
CONSTRUCT ANGLE OFF AXIS SCALE
COMPOSE PARTIAL TITLES FOR PLOT
Y
K=1
N
SYL1 = YL1
SYS1 = YS1
SYL2 = YL2
SYS2 = YS2
SDB(I) = DB (I)
SRP(I) = RP (I)
GO TO 72
K=2
Y
GO TO 2
N
N
IOPT=1
Y
COMPLETE TITLE FOR PLOT
CALL FRAME
CALL PLOT 2
PLOT DB (I), RP(I)
GO TO 72
COMPLETE TITLE FOR AMP PLOT
CALL FRAME
PLOT DB (I)
COMPLETE TITLE FOR PHASE PLOT
CALL FRAME
PLOT RP (I)
GO TO 72

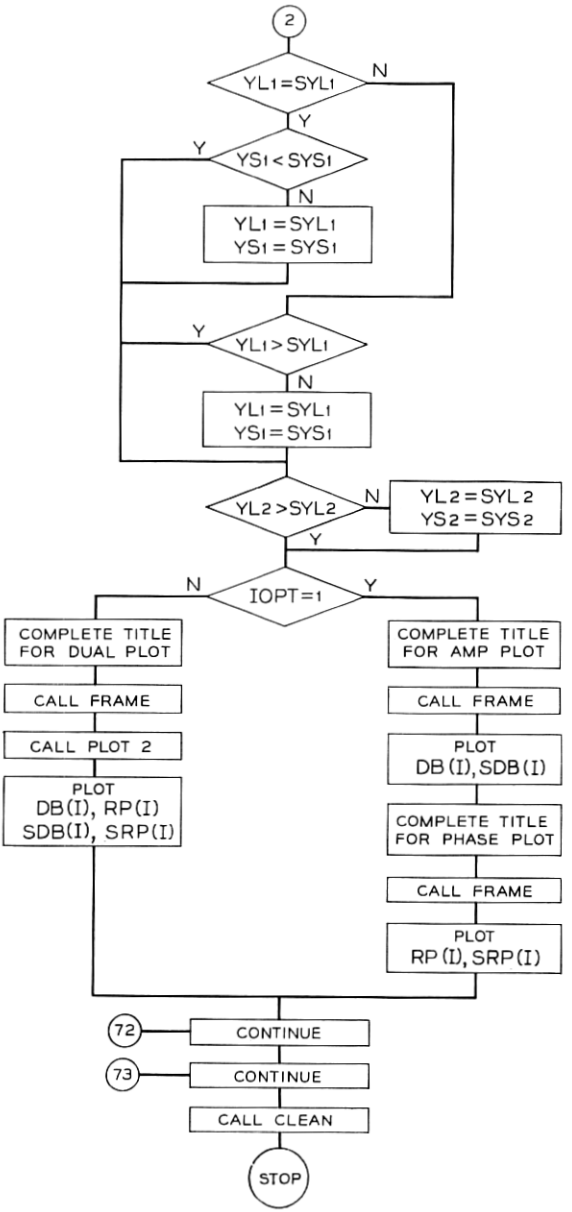


Fig. 23 — Logic diagram for field plotting program.

for the angle-off-axis scale, in degrees, stored in array AS(I):

6.0, 5.0, 4.0, 3.0, 2.5, 2.0, 1.5, 1.0, 0.75, 0.5, 0.4, 0.3, 0.2.

The following subroutines must be included in the deck before execution:

PLOT 2 — A subroutine to generate a grid with two independently labeled ordinates sharing a common abscissa

MINMAX — A subroutine to select the algebraicly largest or smallest entry in an array and specify its index

INTERP — A quadratic interpolation scheme for real arrays

FILTER — Adjusts plotting data for phase variations in the vicinity of $\pm 180°$

LABEL 2 — A modified version of the microfilm subroutine LABEL. Called only by PLOT 2.

The program requires approximately $(51{,}536)_8$ or $(22{,}000)_{10}$ words of storage, and about 0.5 minute execution time for all twelve plots.

ACKNOWLEDGMENTS

The authors gratefully acknowledge the comments and suggestions of J. S. Cook, J. N. Hines, R. Lowell, and E. R. Nagelberg.

REFERENCES

1. Cook, J. S., Elam, E. M., and Zucker, H., "The Open Cassegrain Antenna: Part I—Electromagnetic Design and Analysis," B.S.T.J., *44*, No. 7 (September 1965), pp. 1255–1300.
2. Zucker, H., "Fresnel Region Approximation for Wide Angles and Large Fresnel Numbers," IEEE Trans. Antennas and Propagation, *AP-14* (November 1966), pp. 684–688.
3. Hogg, D. C. and Semplak, R. A., "An Experimental Study of Near Field Cassegrain Antennas," B.S.T.J., *43*, No. 6 (November 1964), pp. 2677–2703.
4. Li, T. and R. H., Turrin, "Near Zone Field of a Conical Horn," IEEE Trans. Antennas and Propagation, *AP-12* (November 1964), pp. 800–802.
5. Potter, P. D., "A New Horn Antenna with Suppressed Sidelobes and Equal Beamwidths," Microwave J. *6* (June 1963), pp. 71–78.
6. Hannan, P. W., "Microwave Antennas Derived from a Cassegrain Telescope," IRE Trans. Antennas and Propagation, *AP-9* (March 1961), pp. 140–153.
7. Silver, S., *Microwave Antenna Theory and Design,* New York: McGraw-Hill, 1949.
8. Alsberg, P. A. and Cochran, J. Alan, unpublished work.